7.2.1 Monocolor barrier layer photoconductor with alloy absorber

The classical nBn barrier layer photoconductor is represented by the N-type AlSbAs/InAsSb barrier–absorber architecture. The barrier layer is selected for approximately zero valence band offset with the absorber InAsSb alloy. $InAs_{0.91}Sb_{0.09}$ is the preferred absorber layer alloy because its lattice constant is consistent with the commonly used GaSb growth substrate. However, growth on GaAs substrates is reported[3] to provide material of equivalent detector quality, indicating that misfit dislocations may not be detrimental to detector dark current performance for the alloy version of the barrier layer photoconductor. The cutoff wavelength of the $x = 0.09$ InAsSb composition is reported[3] to be ~4.1 μm at 150 K. Using the models for dark current and $1/f$ noise developed in Chapters 3 and 4, we can calculate the values of these parameters as a function of operating temperature for any specific nBn architecture. Figure 7.5 illustrates a model of the diffusion current for an $x = 0.09$ InAsSb absorber (a) as a function of doping concentration at 150 K and (b) as a function of inverse temperature for a doping concentration of 5×10^{15} cm^{-3}, assuming that $\tau_{SR} = 400$ ns and an absorber thickness of 3 μm. The optimum donor concentration varies as $\tau_{SR}{}^{1/2}$ but is relatively independent of temperature, and the FPA dark current is seen to equal the $F/3$ flux current at a temperature of ~175 K. At 150 K, the dark current is 2×10^{-7}A/cm^2, in agreement with nBn FPA data.[3]

The systemic $1/f$ noise of an nBn alloy flat-band absorber with an accumulated surface is given by Eq. (4.11a) with the depletion term set to zero:

$$S_{\mathrm{I}}^{\mathrm{dif}} = \left[\frac{q}{2\tau_{\mathrm{Ai1}}} - \frac{q{n_{\mathrm{i}}}^2}{(N+n_{\mathrm{i}})^2\tau_{\mathrm{SR}}}\right]^2 \frac{H^2 N_{\mathrm{T}} A}{f}, \tag{7.1}$$

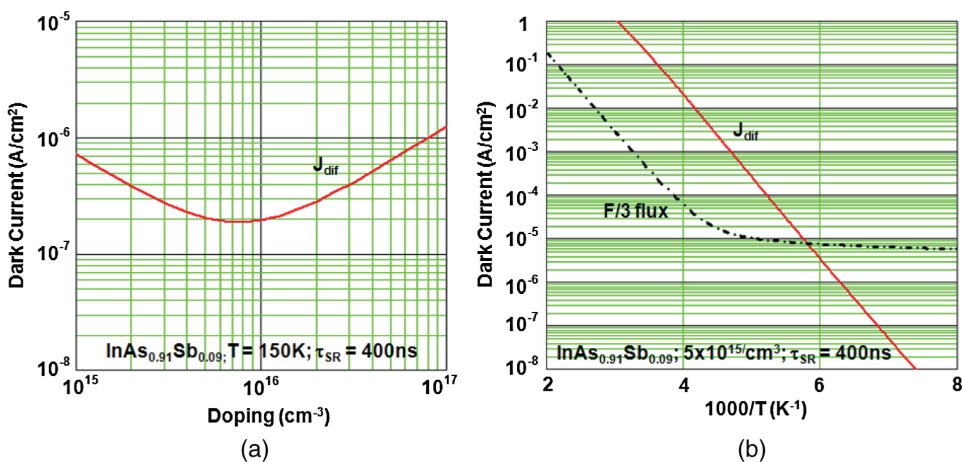

Figure 7.5 (a) Modeled $InAs_{0.91}Sb_{0.09}$ diffusion current versus absorber doping at 150 K for $\tau_{SR} = 400$ ns. (b) Diffusion current versus inverse temperature for a donor doping of 5×10^{15} cm^{-3}.

where H is a parameter that allows for screening of the McWhorter surface trap modulation due to the accumulation layer associated with the mesa-etched and passivated pixel sidewalls. The area A is determined by the mesa etch geometry, and the depth of the mesa is determined by the required MTF and the minority carrier diffusion length in the absorber, which is typically >10 μm at operating temperatures of 150 K. For the purposes of modeling systemic 1/*f* noise in this architecture, it is reasonable to assume a typical etched semiconductor surface trap density of $\sim 10^{12}$ cm^{-2}. A model for the systemic 1/*f* noise figure given by Eq. (7.1) with $H = 1$ as a function of inverse temperature is shown in Fig. 7.6(a) and is compared to the dark current model in Fig. 7.6(b) for the same parameters used in Fig. 7.5. The systemic 1/*f* noise is seen to exceed *F*/3 shot noise at temperatures >170 K, at which point the operability of the FPA will decrease due to systemic noise defects. The temperature dependence of the FPA operability will vary as n_i^2, as will the increase in NETD due to increasing dark current. These predictions are in reasonable agreement with reported data[3] for this specific nBn architecture. No III-V alloy LWIR barrier FPAs have yet been reported, but recent data[1] indicate dark current measurements with a 10-μm-cutoff spectral response for nBn devices fabricated with an $InAs_{0.44}Sb_{0.56}$ absorber at 80 K. The dark current for the 1-μm-thick absorber was 500 μA/cm^2.

7.2.2 Monocolor barrier layer photoconductor with T2SL absorber

The properties and requirements of T2SLs for use as IR photodiodes were discussed in Section 5.2.12. Much of the work in the open literature has addressed the MWIR and LWIR InAs/GaSb versions of this architecture, although, more recently, InAs/InAsSb superlattices have been reported.[9,10]

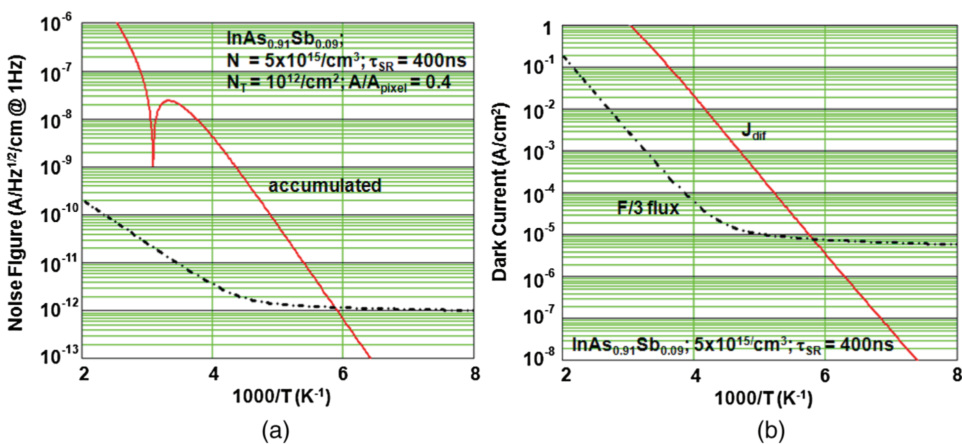

Figure 7.6 Modeled (a) systemic 1/*f* noise figure and (b) dark current versus inverse temperature for an $InAs_{0.91}As_{0.09}$ nBn device with an accumulated surface; $N = 5 \times 10^{15}$ cm^{-3}, $\tau_{SR} = 400$ ns, $N_T = 10^{12}$ cm^{-2}, $A/A_{pixel} = 0.4$, and $H = 1$.

As stated earlier, the operating temperature of all of these diodes is severely limited by the finite values of the S-R lifetime; judged on its own merits, this diode technology is of limited use in the field of IRFPAs. However, the incorporation of T2SLs as absorber layers into the barrier layer photoconductor architecture potentially eliminates the major drawback of depletion current in the absorber volume, enabling considerably higher operating temperatures in much the same manner as for the nBn architecture utilizing alloy absorbers. The T2SL offers the added benefit of a capability to eliminate Auger generation by minimizing the phase space available for Auger transitions. This not only results in an absence of Auger-limited diffusion current but theoretically allows for the use of even larger doping concentrations, albeit consistent with in-plane and perpendicular tunneling considerations, and thus a subsequent reduction in S-R limited diffusion current.

It should be pointed out also that, with regard to using T2SL technology in the barrier layer photoconductor architecture, the formation of minority carrier barriers with zero offsets is greatly facilitated by an appropriate selection of layer geometries and alloy content, consistent with approximate lattice matching to the growth substrate. As stated earlier, the conduction band edge is determined primarily by the width of the InAs layers, and the heavy-hole valence band edge is determined by the width of the GaSb layers, allowing for relatively easily designed band edge alignments. The required barrier heights for majority and minority carriers in complementary barrier structures are generated either by the use of thinner layers of the relevant constituent layer or by utilizing a larger-bandgap lattice-matched alloy. This is unlike the nBn alloy absorber case in which one is limited to the band offsets and lattice constants provided by nature.

There are many variations of the T2SL absorber theme reported in the literature, but we will simply model dark current and $1/f$ noise for the generic barrier–absorber case, assuming an absence of minority carrier injection from the majority carrier contact and zero majority carrier flow over the majority carrier barrier. In keeping with the preponderance of reported data in the literature, we will consider the absorber and barrier to be P type due to the preference for the relatively mobile electron as the minority carrier. The collector contact is to a large extent irrelevant but will be assumed to be P type to avoid any tendency to form a depletion region at the barrier–absorber interface. This architecture will require an applied bias voltage on the collector contact to initiate minority carrier flow but at the same time will enable non-equilibrium operation of the absorber without the formation of a depletion region. Considering the LWIR case with Auger7 suppression and flat-band absorber operation, with accumulated surfaces, the only relevant dark current component is S-R diffusion current, given by

$$J_{\mathrm{dif}}^{\mathrm{SR}} = \frac{q n_{\mathrm{i}}^{2} t}{(P + n_{\mathrm{i}})\tau_{\mathrm{SR}}}, \tag{7.2}$$

and the systemic $1/f$ noise is given by Eq. (7.1) without the Auger term:

$$S_{\mathrm{I}} = \left[-\frac{q n_{\mathrm{i}}^{2}}{(P + n_{\mathrm{i}})^{2} \tau_{\mathrm{SR}}} \right]^{2} \frac{N_{\mathrm{T}} A_{\mathrm{dif}}}{f}. \tag{7.3}$$

Figure 7.7 shows the modeled dark current and systemic $1/f$ noise for the above straw-man pBp barrier layer photoconductor as a function of inverse temperature, given by Eqs. (7.2) and (7.3). For the purposes of the model, we have assumed that $P = 10^{16}$ cm^{-3}, $\tau_{\mathrm{SR}} = 40$ ns, $t = 2$ μm, $N_{\mathrm{T}} = 10^{12}$ cm^{-2}, and a 30-μm-pixel pitch and have compared them to $F/2$ flux current and shot noise. The predicted dark current and systemic $1/f$ noise both exhibit a n_{i}^{2} temperature dependence. It is apparent that the NETD of an LWIR FPA based on this architecture should be background limited at 80 K for the assumed idealized conditions.

There are a number of potential issues with regard to the use of P-type absorbers in any semiconductor materials system, not the least of which is the sensitivity of surfaces to fixed charge, which is typically positive in nature, and the problems created by dislocations, which are routinely considered as highly charged donor pipes. The former can generate both excess current and systemic $1/f$ noise, whereas the latter will generate excess current and isolated defect $1/f$ noise. It is relatively straightforward to model the effect of fixed positive charge in the form of a depleted sidewall surface on the dark current and systemic $1/f$ noise plots of Fig. 7.7 by the inclusion of a surface depletion current term. The dark current is now given by

$$J_{\mathrm{dark}} = \frac{q n_{\mathrm{i}}^{2} t}{(P + n_{\mathrm{i}}) \tau_{\mathrm{SR}}} + \frac{q n_{\mathrm{i}} W 4t}{\tau_{\mathrm{SR}} L}, \tag{7.4}$$

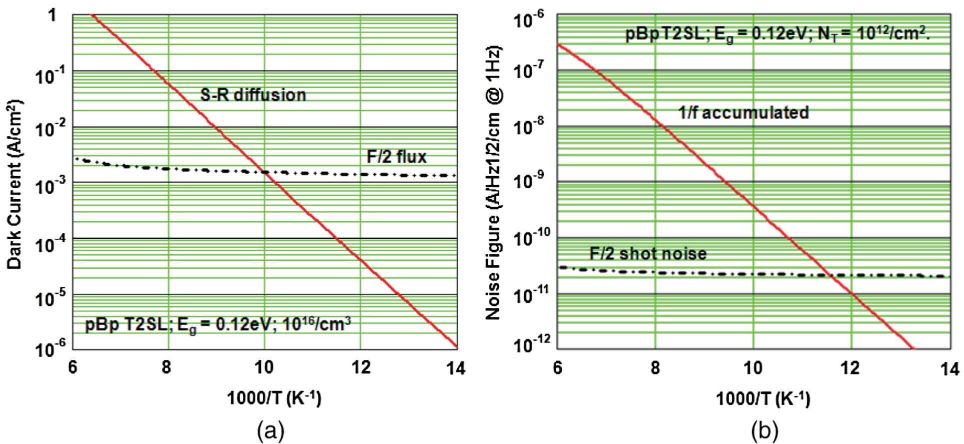

Figure 7.7 (a) Dark current and (b) systemic $1/f$ noise as a function of inverse temperature for a LWIR pBp barrier layer photoconductor, assuming Auger7 suppression, flat-band absorber operation, and accumulated surfaces; $P = 10^{16}$ cm^{-3}, $\tau_{\mathrm{SR}} = 40$ ns, 30-μm pixel, and $t = 2$ μm.

where W is the width of the surface depletion region, and L is the pixel pitch. The systemic $1/f$ noise figure is given by Eq. (4.13), less the Auger7 term, as

$$S_{\mathrm{I}} = \left[\frac{qn_{\mathrm{i}}}{\tau_{\mathrm{SR}}} - \frac{qn_{\mathrm{i}}^2}{(P+n_{\mathrm{i}})^2\tau_{\mathrm{SR}}}\right]^2 \frac{N_{\mathrm{T}}A}{f}. \tag{7.5}$$

The depleted surface case of the pBp T2SL architecture is shown in Fig. 7.8, utilizing Eqs. (7.4) and (7.5), and compared to the previously considered accumulated surface condition. As expected, there is a significant increase in both dark current and systemic $1/f$ noise at 80 K, although the dark current still remains less than the *F*/2 flux current at 80 K.

Test diode data have been reported[12] by the JPL group on a complementary-barrier IR detector (CBIRD) architecture that employs a similar hole barrier–absorber interface to the straw man considered in Fig. 7.7 and 7.8, but with an *N*-type collector contact structure. The better test diode data are in excellent agreement with the accumulated surface case considered in Fig. 7.7 and exhibit an n_{i}^2 temperature dependence. However, other dark current data by JPL[13] on a CBIRD 320 × 256 30-μm-pitch LWIR FPA with similar architecture exhibits significantly higher mean dark current of ~220 μA/cm^2 at 78 K, although this value is still low enough to enable an NETD of ~18.6 mK at that temperature. This dark current is consistent with a contribution due to surface depletion current, as previously described. The NETD of this FPA is reported to improve to 12 mK at an operating temperature of 65 K, indicating that the dark current is indeed mildly temperature dependent at the operating bias of 0.128 V. A further analysis[14] of dark current as a function of both temperature and bias, taken on this FPA and its associated 200-μm test diode process evaluation chips, revealed a

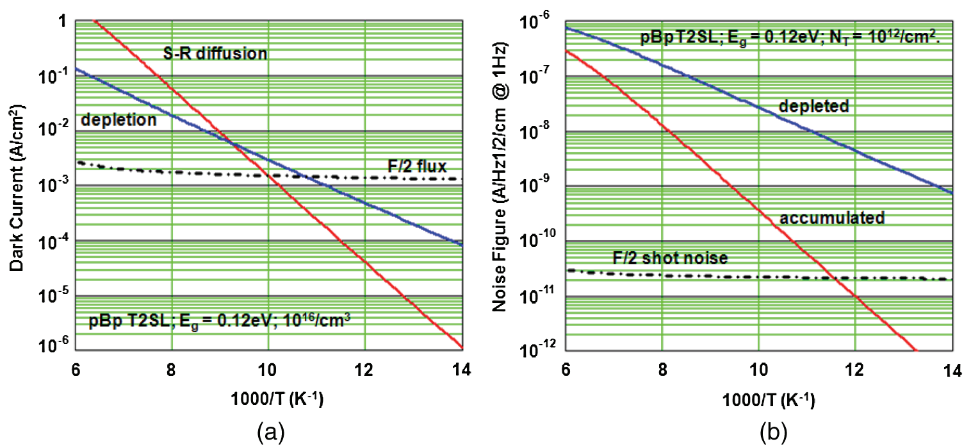

Figure 7.8 Models for (a) dark current and (b) $1/f$ noise figure versus inverse temperature for a 2-μm-thick LWIR pBp T2SL absorber with a 30-μm pixel and depleted and accumulated surfaces.